c-axis electrical conductivity and thermoelectric power of sodium hydride–graphite ternary intercalation compounds

Toshiaki Enoki, Noriaki Sakamoto, Keisuke Nakazawa, and Kazuya Suzuki
Department of Chemistry, Tokyo Institute of Technology, Ookayama, Meguro-ku, Tokyo 152, Japan

Ko Sugihara and Koji Kobayashi
College of Pharmacy, Nihon University, Narashinodai, Funabashi 274, Japan
(Received 8 July 1992; revised manuscript received 20 November 1992)

The electronic structures of sodium hydride intercalated graphite (NaH-GIC's) $C_{an}NaH$ ($a=2.5$–4.5, $n=$stage index), which have ionic triple atomic layers Na^+-H^--Na^+ in their graphitic galleries, are investigated using *c*-axis resistivity and thermoelectric power measurements. The introduction of NaH in the graphitic galleries depresses the *c*-axis resistivity, in contrast to the case of the isostructural compounds KH-GIC's or KHg-GIC's. This suggests that the NaH intercalate does not contribute to the transport properties. The thermoelectric power, which is explained mainly in terms of phonon-drag effects, anomalously decreases as the stage index increases. This behavior is explained by the important role played by the domain-scattering mechanism of phonons in phonon-drag effects, and proves that the Fermi surface of graphitic π electrons is small. The results of thermoelectric power measurements give the Fermi energy at $E_F=0.45$ eV for a stage-3 compound, which is considerably smaller than that for KHg-GIC's and KH-GIC's. From these experimental results, it is suggested that the ionic NaH intercalate with a stoichiometric composition of [Na]/[H]=1 makes a complete charge transfer within the intercalate layer, resulting in the presence of a small concentration of graphitic π-electron carriers and the absence of conduction carriers in the intercalate regions.

INTRODUCTION

Graphite is a layered material with a conduction π-electron system. Graphitic galleries are available to intercalate foreign species, leading to the formation of graphite intercalation compounds (GIC's).[1,2] GIC's with additional layers in every graphitic gallery are called stage-1 compounds, while those with one added layer per n graphitic galleries are stage-n compounds. Among GIC's, alkali-metal GIC's, whose stoichiometries are C_8M for stage-1 and $C_{12n}M$ for stage-n compounds (M=K, Rb, and Cs), are known to absorb hydrogen in the graphitic galleries through either chemisorption or physisorption processes.[3–7] In the high-temperature region above about 200 K, chemisorbed hydrogen species are stabilized in the intercalate space through the dissociation of hydrogen molecules and through the charge-transfer process from the host alkali-metal GIC to hydrogen.[3–5] At low temperatures below about 200 K, hydrogen molecules are occluded by physisorption without any dissociation process.[6,7] The hydrogen-chemisorbed alkali-metal GIC's, which are regarded as alkali-metal hydride GIC's, are systems analogous to transition-metal hydrides such as PdH_x or VH_x,[8,9] while the hydrogen-physisorbed systems are considered to be similar to molecular sieves such as activated charcoal or zeolites.[7]

We have been interested mainly in the electronic properties and structures of the hydrogen-chemisorbed GIC's, from the viewpoint of metal-hydrogen systems.[10–21] The hydrogen chemisorption strongly depends on the alkali metals, and the magnitude of the chemisorption activity decreases in the order of $K>Rb>Cs$.[3,5] In a K-GIC, hydrogen is accommodated in interstitial sites of the potassium lattice in the intercalate space at low hydrogen concentration $x<0.1$ for C_8KH_x, while an additional introduction of hydrogen induces a structural change to a stage-2 compound where the introduced hydrogen forms a layered lattice sandwiched between two potassium atomic layers in the graphitic galleries.[4,5,22] The Cs-GIC has no activity for hydrogen chemisorption, even though it shows strong catalytic activity for the hydrogen-deuterium exchange reaction.[23] The activity in a Rb-GIC is intermediate between them.[3,4] At ambient hydrogen pressure, the hydrogen concentration becomes saturated only at $x=0.05$ and the application of pressure up to about 100 atm is required to reach a hydrogen concentration $x=0.67$, where the formation of the stage-2 structure analogous to $C_8KH_{0.67}$ is completed.[3] The direct intercalation of alkali hydrides into graphite can also give alkali-metal hydride GIC's similar to the materials obtained by hydrogen chemisorption. In the case of KH-GIC's, the direct intercalation of KH gives compounds with stoichiometries of $C_{4n}KH_x$ (stage number $n=1,2$, $x=0.8$),[24,25] which have a higher hydrogen concentration than that obtained by hydrogen absorption. We can also prepare RbH-GIC's and CsH-GIC's by direct intercalation,[26] though these compounds are less stable than their KH analogs. Sodium hydride GIC's are special among alkali-metal hydride GIC's. It is difficult to prepare Na-GIC's except for compounds with stages higher than stage 4.[1] However, the direct intercalation of NaH can provide NaH-GIC's with anomalous

stoichiometries of $C_{an}NaH$ ($a=2.5-4.5$).[27,28]

It is well known that there are two kinds of metal-hydrogen systems. Transition-metal hydrides, which are typical metal-hydrogen systems, are considered to be metal-hydrogen alloys where hydrogen has a delocalized electronic nature,[8,9] while alkali-metal hydrides such as K^+H^- are ionic insulators having hydrogen anions H^- with a localized electronic state. The electronic structure of KH-GIC's investigated by measurement of the specific heat,[10,11] Shubnikov–de Haas oscillations,[12] and optical reflectance[29] is characterized by the ionic sandwiched triple atomic layers K^+-H^--K^+ intercalated between metallic graphitic sheets. This suggests that the electronic structure of the intercalated hydrogen has a nature similar to pristine KH. However, detailed investigations with proton NMR,[13,14,30] thermoelectric power,[15] photoemission spectroscopy,[16] and magnetoresistance[19] demonstrate the presence of two-dimensional metallic hydrogen layers[31,32] in the graphitic galleries, which is accomplished by the incomplete charge transfer from the host K-GIC to hydrogen H^- and the nonstoichiometric ratio of $[H]/[K]=0.67\sim0.8$. Therefore these experimental facts suggest that the electronic properties of the hydrogen in KH-GIC's is between that in transition-metal hydrides and that in alkali-metal hydrides. NaH-GIC's, which are discussed in this paper, have more ionic structure than KH-GIC's and the ratio between Na and H is almost unity.[27,28] The difference in the structures between these two alkali-metal hydride GIC's will give the hydrogen in NaH-GIC's a different electronic nature from that of hydrogen in KH-GIC's.

In this paper we investigate the electronic structure of NaH-GIC's by means of *c*-axis resistivity and thermoelectric power measurements.

EXPERIMENTAL DETAILS AND RESULTS

Sodium hydride–graphite ternanry compounds with stoichiometries $C_{an}NaH$ ($a=2.5-4.5$) for stage-*n* structures were prepared by the direct intercalation of sodium hydride[27] into highly oriented pyrolytic graphite (HOPG, Union Carbide) flakes. Sodium hydride powder and HOPG flakes sealed in a glass vacuum tube were heat treated at 400–500 °C for one to several days to obtain stage-2 to stage-6 NaH-GIC's. Samples were characterized with (001) x-ray-diffraction patterns before electrical measurements. The *c*-axis repeat distances are identical to those reported by Guérard *et al.*[27] ($I_c=14.2$, 17.6, 20.9, and 24.3 Å for stage-3 to stage-6 compounds). The *c*-axis resistivity was measured by means of the dc four-probe technique from liquid-helium temperature to room temperature. The thermoelectric power was measured by the technique developed by Chaikin and Kwak[33] with AuFe Chromel thermocouples in the temperature range from 4.2 K to room temperature. The temperature was monitored by Ge ($T<35$ K) and Pt ($T>35$ K) thermometers.

The temperature dependences of the *c*-axis resistivities are shown in Fig. 1 for stage-3 to stage-6 samples. The resistivities showed metallic behavior for all compounds with different stages, even though the magnitudes of the

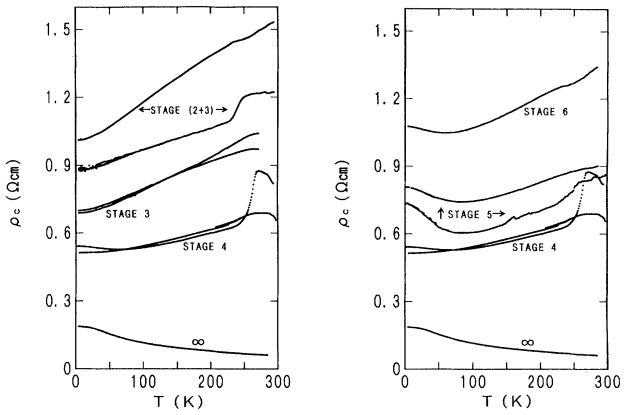

FIG. 1. Temperature dependence of the *c*-axis resistivity ρ_c for stage-3 to stage-6 NaH-GIC's. ∞ denotes the resistivity for pristine HOPG. Stage (2+3) is a sample with a mixture of stage 2 and stage 3.

resistivities are relatively high, ranging from 0.5 to 1.5 Ω cm and showing a stage dependence, where the resistivities are a minimum at a stage-4 compound. The large resistivity values suggest that the *c*-axis conduction is attributed to a hopping process in NaH-GIC's. For the compounds with stage number higher than stage-4, an increase in resistivity is observed at low temperatures below about 70 K. The anomalous changes in the resistivities shown just below room temperature in stage-(2+3) and stage-4 compounds might be associated with a degradation process taking place at high temperatures above about 250 K.

The temperature dependence of the thermoelectric power parallel to the *ab* plane, S_a, is shown in Fig. 2 for

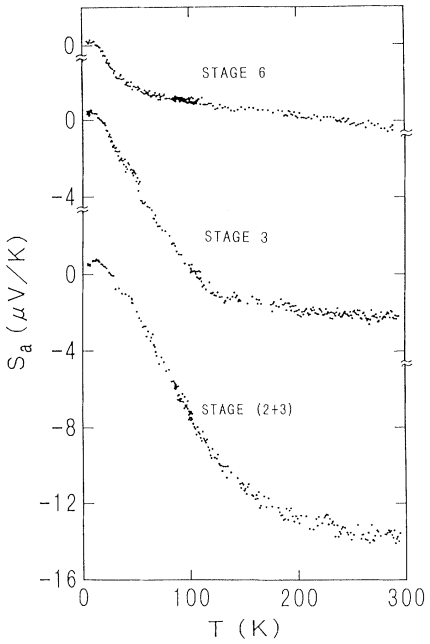

FIG. 2. Temperature dependence of the in-plane thermoelectric power S_a for stage-(2+3), stage-3, and stage-6 NaH-GIC's.

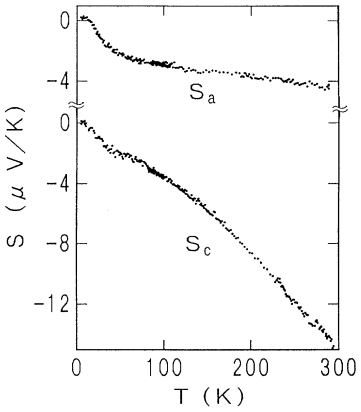

FIG. 3. Temperature dependence of the in-plane and c-axis thermoelectric powers, S_a and S_c, for a stage-6 NaH-GIC.

stage-(2+3), stage-3, and stage-6 compounds. The thermoelectric power has negative values over the whole temperature range, except at low temperatures below about 20 K for all compounds. This finding suggests that the majority of carriers are associated with the graphitic π electrons which are generated by the charge transfer from NaH ionic donor intercalate to graphite. In the mixed-stage compound [stage-(2+3)], the thermoelectric power increases slowly as the temperature is lowered from room temperature. Below about 100 K, the thermoelectric power increases steeply and finally changes sign to positive values below about 20 K. The stage-3 sample shows a trend similar to the stage-(2+3) sample, although it has a kink at 120 K. The thermoelectric power vs temperature curve of the stage-6 NaH-GIC sample has a weak temperature dependence above about 40 K and shows a steep increase below that temperature. Figure 3 shows the temperature dependence of the c-axis thermoelectric power S_c for the stage-6 compound in comparison with the in-plane thermoelectric power S_a. S_c, which is negative over the whole temperature range, has an approximately linear temperature dependence with a weak anomaly around 40 K, at which S_a shows a change in trend. Overall, S_c has larger absolute values than S_a. A positive contribution, which is observed in the S_a trace below about 20 K, is absent in the behavior of S_c.

DISCUSSION

Now we discuss the c-axis resistivities with particular reference to the anomalous temperature and stage dependences that are observed. c-axis resistivities with magnitudes around 1 Ω cm are very much larger than those for the isostructural KHg-GIC's (Ref. 34) and KH-GIC's.[15] The c-axis conduction with resistivity values of 10^{-2}–10^{-3} Ω cm in KHg-GIC's, which have alloy intercalates consisting of K-Hg-K triple atomic layers, is situated close to the borderline between band conduction ($l_c > I_c$) and hopping conduction ($l_c < I_c$), where l_c and I_c are the mean free path of carriers parallel to the c axis and the c-axis repeat distance, respectively. KH-GIC's are considered to have a hopping mechanism for c-axis conduction, since they have larger c-axis resistivity values (10^{-1}–10^{-2} Ω cm) than KHg-GIC's. Taking these facts into account, it is suggested that the c-axis transport can be explained by a hopping conduction mechanism in NaH-GIC's, whose resistivity values are two or three orders of magnitude larger than those of the isostructural KHg-GIC's.

Since GIC's have stacking structures with a sequence of graphene double layer units and graphene-intercalate-graphene composite layer units, the c-axis resistivities of a stage-n compound (stage index n) can be analyzed phenomenologically on the basis of the equation

$$\rho_c = (1/n)[\rho_{c,\mathrm{GIG}} + (n-1)\rho_{c,\mathrm{GG}}] , \quad (1)$$

where $\rho_{c,\mathrm{GG}}$ and $\rho_{c,\mathrm{GIG}}$ denote the resistivity contributions from the graphene double layer unit and the graphene-intercalate-graphene composite layer unit, respectively. Using Eq. (1) with experimental results of the stage-dependent resistivities, these two contributions are estimated to be $\rho_{c,\mathrm{GIG}} \sim 3$ Ω cm and $\rho_{c,\mathrm{GG}} < 1$ Ω cm at room temperature. Namely, the ratio of $\rho_{c,\mathrm{GG}}$ to $\rho_{c,\mathrm{GIG}}$ is less than unity; $\rho_{c,\mathrm{GG}}/\rho_{c,\mathrm{GIG}} < 0.3$. This means that the introduction of the NaH intercalate decreases the c-axis conduction. In other words, the NaH intercalate layers do not contribute to the c-axis transport. The trend in NaH-GIC's is different from other isostructural analogs, KH-GIC's and KHg-GIC's, with $\rho_{c,\mathrm{GG}}/\rho_{c,\mathrm{GIG}} = 14$ and 7, respectively. As mentioned above, in KHg-GIC's and KH-GIC's there exists conduction carriers in the intercalate layers as well as the graphitic π-conduction carriers; carriers of the KHg alloy intercalates for the former and hole carriers on the two-dimensional metallic hydrogen lattice for the latter. Therefore we can suggest that there are no NaH intercalate carriers in NaH-GIC's, different from KHg-GIC's and KH-GIC's. Figure 4 shows the stage dependence of the c-axis resistivities at room temperature and 4.2 K from stage-1 to stage-6 compounds, where we employ $\rho_{c,\mathrm{GIG}}$ as the resistivity value for the stage-1 compound. c-axis resistivities decrease with increasing stage index until stage 4, which has the minimum resistivity; above stage 4 the c-axis resistivities are again elevated. The increase in c-axis resistivities for lower-stage compounds suggests the absence of conduc-

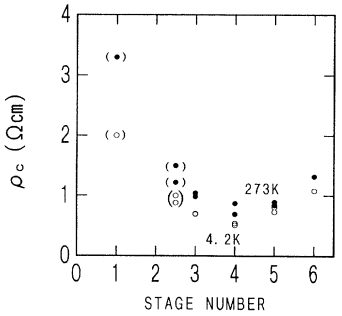

FIG. 4. Stage dependence of the c-axis resistivity ρ_c at 4.2 (○) and 273 K (●) in NaH-GIC's. The data in parentheses are the values obtained after analysis for stage 1 or the data for mixed stage (2+3).

tion carriers on the NaH intercalate in the graphitic galleries. Structures of higher-stage GIC's are known to have stacking faults, which contribute to carrier scattering for the c-axis conduction.[35] The increase in ρ_c for higher-stage compounds can be attributed to the carrier scattering by stacking faults.

Next we discuss the temperature dependence of the c-axis resistivities. The trend in the temperature dependence of the c-axis resistivities is metallic, even though the magnitudes of ρ_c are in the hopping conduction range ($1_c \ll I_c$). The residual resistivity ratio ranges from about 0.5 to 1, depending on the stage index. As Sugihara suggested,[36,37] the c-axis conduction includes two processes. A carrier stays on a graphitic plane between successive hopping events. In the graphitic plane, the carrier transport is governed by in-plane phonon scattering, resulting in a relaxation time similar to that observed for the in-plane resistivity. The hopping between graphitic planes occurs with the assistance of impurities and (001) phonons, the former contributing mainly to the conduction process. The expression for the conductivity, considering the two scattering processes available to low-state compounds, is given by the equation

$$\sigma_c = \frac{e^2 N \Omega_0 I_c}{2\hbar} \frac{2E_F}{3\gamma_0 b} \frac{|J|^2}{\Gamma} , \tag{2}$$

where N, Ω_0, E_F, J, γ_0, b, and Γ are the carrier density, the unit cell volume, the Fermi energy, the interplanar interaction associated mainly with impurity-assisted hopping, the graphitic in-plane band parameter (3.16 eV), the in-plane C-C atomic distance (1.42 Å), and the relaxation time of the in-plane carrier scattering, respectively. Since Γ has a metallic temperature dependence similar to that for the in-plane resistivities, it is assumed that the metallic temperature dependence observed for low-stage compounds (at least below stage 4) is associated with the in-plane carrier scattering, which also affects the c-axis hopping conduction.

In the present experiments, metallic behaviors in the temperature dependence of ρ_c are also observed for higher-stage compounds, although the scattering by stacking faults, which give an activation-type behavior in ρ_c, overwhelm other scattering mechanisms in the higher-stage compounds, as suggested in Fig. 4. This finding is curious and is in disagreement with results observed in high-stage (stage-5) K-GIC, where the temperature dependence is consistent with an activation mechanism, except in the low-temperature range. The second anomalous point concerns the increase in ρ_c in the low temperature range below about 70 K for higher-stage compounds (stage 5 and stage 6). One possibility to explain this is to assume that the scattering by stacking faults follows an activation mechanism, though the behavior is not in agreement with that predicted by Sugihara.[36] The next possibility concerns carrier localization.[39] Since higher-stage compounds have structures with smaller domains formed in the intercalation reaction (Daumas-Hérold domain),[38] the presence of disorder might contribute to the localization of carriers. Yet another possibility is related to the presence of localized spins. NaH-GIC's (especially those higher than stage 1) have anomalously broad electron-spin-resonance (ESR) spectra (linewidth $\sim$60 G) even though the small spin-orbit interactions of the constituent elements are expected to result in a sharp linewidth. The temperature dependence of the magnetic susceptibility obeys Curie's law, suggestive of the presence of localized spins as well as the graphitic conduction π-electron spins.[27] Since the NaH ionic intercalate is expected to have defect centers with localized spins such as F centers, the electrons weakly bound at the defect centers have expanded orbitals, so that the ESR signal becomes broad due to the effect of hyperfine interactions from surrounding Na and H atoms. The exchange coupling between the localized spins and the graphitic conduction π-electron spins generates a broad asymmetric ESR signal. The presence of the localized spins in the NaH intercalates interacting with the conduction electrons can give rise to enhanced resistivities at low temperatures.[40]

With regard to the discussion of the thermoelectric power, as mentioned above, the main contribution is ascribed to the π electrons in the graphitic π^* conduction bands, which have electron character. There are two characteristic behaviors observed in the in-plane thermoelectric power S_a in NaH-GIC's. The thermoelectric power tends to saturate in the high-temperature range for all of the samples with stage (2+3) to stage 6. The absolute values of the thermoelectric power decrease with increasing stage index, as opposed to the trend in ordinary GIC's with π electrons as the majority carriers.[41] The thermoeletric power is explained in terms of the electron diffusion process (S_d) and the phonon-drag process (S_p). The former contribution gives a linear temperature dependence in the in-plane thermoelectric power S_a, which is expressed by the equation[41,42]

$$S_{ad,i} = \frac{\pi^2 k_B^2}{3e} T \left[\frac{\partial \ln \sigma_{a,i}}{\partial E} \right]_{E_F} , \tag{3}$$

where i is a band index for the conduction carriers and the contribution of carriers in the ith band to the in-plane conductivity is given as

$$\sigma_{a,i} = \frac{N_i e^2 \tau_i v_{F,i}}{\hbar k_{F,i}} , \tag{4}$$

in which N_i is the carrier density for the ith graphitic band, which is approximated by a cylindrical Fermi surface having an in-plane wave number $k_{F,i}$,

$$N_i = \frac{k_{F,i}^2}{\pi I_c} , \tag{5}$$

and $v_{F,i}$ is the Fermi velocity,

$$v_{F,i} = \frac{1}{\hbar} \left[\frac{\partial E_i}{\partial k} \right]_{E_F} . \tag{6}$$

Here τ_i represents the in-plane relaxation time with the energy dependence[41,43]

$$\tau_i(E) = \tau_{0i} E^{P_i} . \tag{7}$$

The value of P_i is given to be -1 or 0 for the relaxation

time associated with the acoustic phonons in a two-dimensional electronic system with a linear or a parabolic energy dispersion, respectively. The phonon-drag term has characteristic behavior, showing a saturation at high temperatures in GIC's, which is related to the phonon-scattering mechanism. Equation (8) gives an expression for the phonon-drag term in the in-plane thermoelectric power:[41,42]

$$S_{ap,i}=\frac{\langle C_{p,i}R\rangle_i}{2eN_i} , \tag{8}$$

where $C_{p,i}$ denotes the specific heat of the phonon system, which can interact with the π electrons in the ith band. R is the momentum-transfer ratio through the electron-phonon interaction from the phonon system to carriers, and the q dependence of R is given by[41,42]

$$R=\frac{t}{t_c}=\frac{aq}{B+aq+fq^3+AqT^3} , \tag{9}$$

where $1/t$ is the total phonon relaxation rate, which includes processes of (1) the electron-phonon scattering ($aq=1/t_c$), (2) the boundary scattering (B), (3) the Rayleigh scattering associated with point defects and vacancies, and also due to the strain-field scattering (fq^3), and (4) the phonon-phonon scattering (AqT^3). The boundary scattering is related to the domain size L as $B=v_s/L$, where v_s is the sound velocity of the acoustic phonons. In GIC's, the introduction of guest species into the graphitic galleries in an intercalation reaction forms domain structures (Daumas-Hérold domains), depending on stage indices.[38] The Rayleigh scattering, the electron-phonon scattering, and the phonon-phonon scattering all depend on the phonon momentum q, so that the shape and the size of the Fermi surfaces affect the behavior of R and of the phonon-drag term through these scattering processes since the momentum of phonons available to these processes is cut off at $q=2k_F$.

Here we analyze the experimental data for the in-plane thermoelectric power for the stage-3 compound in order to investigate the temperature dependence of the thermopower and to extract information on the electronic structure. (The stage-6 compound has six conduction bands, so that analysis is complicated.) According to the Blinowski and Rigaux model,[45] the stage-3 compound has three conduction π bands ($1c$, $2c$, and $3c$), to which electrons in the NaH intercalates are transferred, as shown in Eqs. (10)–(12) and Fig. 5,

$$E_1=|\tfrac{3}{2}\gamma_0 bk| , \tag{10}$$

$$E_2=[\gamma_1^2+\tfrac{9}{4}\gamma_0^2b^2k^2-(\gamma_1^4+\tfrac{9}{2}\gamma_0^2\gamma_1^2b^2k^2)^{1/2}]^{1/2} , \tag{11}$$

$$E_3=[\gamma_1^2+\tfrac{9}{4}\gamma_0^2b^2k^2+(\gamma_1^4+\tfrac{9}{2}\gamma_0^2\gamma_1^2b^2k^2)^{1/2}]^{1/2} , \tag{12}$$

where b is the in-plane C-C distance (1.42 Å), and the intralayer and interlayer resonance integrals are denoted by $\gamma_0=3.16$ eV and $\gamma_1=0.39$ eV, respectively. [In these equations, we neglect the potential-energy difference among graphitic layers since the concentration of charge transferred to the graphitic layers is expected to be small as mentioned before, namely, $\delta=0$ in Eq. (9) in Ref. 45.]

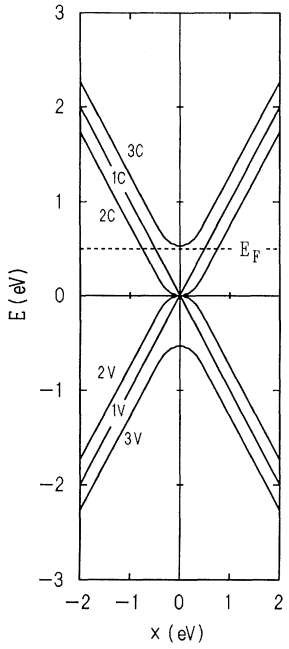

FIG. 5. Band structure of stage-3 NaH-GIC on the basis of the Blinowski and Rigaux model ($\delta=0$). The units of the abscissa are $x=\frac{3}{2}\gamma_0 bk$. $1c$, $2c$, and $3c$ denote conduction bands while $1v$, $2v$, and $3v$ are valence bands. E_F is estimated at 0.45 eV from the analysis of the thermoelectric power data.

The band $1c$ has a linear energy dependence, while the energy dispersions of the bands $2c$ and $3c$ are approximately expressed as parabolic functions in the low-energy region below about $|E|<0.5$ eV. Figure 5 shows that the bottom of the conduction band $3c$ is shifted up by $\sqrt{3}\gamma_1=0.54$ eV from the bottoms of the bands $1c$ and $2c$. As shown in the discussion below, the Fermi energy E_F is below about 0.5 eV, so that only bands $1c$ and $2c$ are occupied by the electrons transferred from the NaH intercalates. Therefore we need not take into account the contribution of band $3c$ to the thermoelectric power.

First, we calculate the electron diffusion term S_{ad} according to Eq. (3). The contribution of the band $1c$ to the electron diffusion term is given using Eqs. (3)–(7) and (10), as follows:

$$S_{ad,1}=\frac{\pi^2k_B^2}{3e}\frac{1+P_1}{E_F}T , \tag{13}$$

where the exponent in the energy dependence of the relaxation time $\tau_1(E)$ associated with the acoustic phonons is given by $P_1=-1$ for the band with the linear energy dispersion.[41] The electron diffusion term for band $2c$ with a parabolic energy dispersion, which is calculated by Eq. (11), has a form identical to Eq. (13) for band $1c$, although the energy dependence of the relaxation time $\tau_2(E)$ gives $P_2=0$ for the parabolic band coupled with the acoustic phonons.[43,44]

Next, we calculate the phonon-drag terms for both

bands. The electron-phonon terms for bands 1c and 2c are expressed by the equations[41–44]

$$a_1 q = \frac{\hbar D^2}{\pi I_c d}\left[\frac{4k_{F,1}}{9\gamma_0^2 b^2}\right]q \ , \tag{14}$$

$$a_2 q = \frac{\hbar D^2}{\pi I_c d}\left[\frac{m_2^*}{\hbar^2}\right]^2 \frac{1}{k_{F,2}} q \ , \tag{15}$$

where D is the deformation potential for the graphitic π electrons having the magnitude of $D=16$ eV, m_2^* is the effective mass for band 2c, and d is the crystal density. In Eq. (8), $\langle C_{p,i} R \rangle_i$ is given for $i=1$ or 2 as

$$\langle C_{p,i} R(q) \rangle_i = \frac{1}{2\pi I_c}\int_0^{2k_{F,i}} dq\, q \frac{(\hbar\omega_q)^2}{k_B T^2} N_q (N_q+1) R(q) \ , \tag{16}$$

where N_q is the equilibrium in-plane acoustic phonon distribution. If we take $x=\hbar v_s q/k_B T$ and $x_{\max,i}=2\hbar v_s k_{F,i}/k_B T$, using Eq. (16), the phonon-drag term is given by the equation

$$S_{ap,i} = \frac{k_B^3}{4ek_{F,i}^2\hbar^2 v_s^2} T^2 \int_0^{x_{\max,i}} dx\, x^3 \frac{e^x}{(e^x-1)^2} R(x) \ , \tag{17}$$

where $R(x)$ is expressed by the following equation for band 2c, using Eq. (15):

$$R(x) = \frac{k_B T}{\hbar v_s}\frac{\hbar D^2}{\pi I_c d}\left[\frac{m_2^*}{\hbar^2}\right]^2 \frac{1}{k_{F,2}} \frac{x}{\frac{v_s}{L}+\frac{\hbar D^2}{\pi I_c d}\left[\frac{m_2^*}{\hbar^2}\right]^2\frac{1}{k_{F,2}}\left[\frac{k_B}{\hbar v_s}\right]xT + f\left[\frac{k_B}{\hbar v_s}\right]^3 x^3 T^3 + A\left[\frac{k_B}{\hbar v_s}\right]xT^4} \ . \tag{18}$$

The expression for band 1c can be derived by replacing $(m_2^*/\hbar)^2$ with $2k_{F,1}/3\gamma_0 b$.

The observed in-plane thermoelectric power includes contributions from the two bands as given by the equation

$$S_a = \frac{\sum_{i=1}^{2} \sigma_{a,i}(S_{ad,i}+S_{ap,i})}{\sum_{i=1}^{2}\sigma_{a,i}} \ , \tag{19}$$

which is modified by the total electron diffusion term S_{ad} and the total phonon-drag term S_{ap} as follows:

$$S_a = S_{ad}+S_{ap} = \frac{S_{ad,1}\sigma_{a,1}+S_{ad,2}\sigma_{a,2}}{\sigma_{a,1}+\sigma_{a,2}} + \frac{S_{ap,1}\sigma_{a,1}+S_{ap,2}\sigma_{a,2}}{\sigma_{a,1}+\sigma_{a,2}} \ . \tag{20}$$

Using Eq. (13), the following expression is obtained for the total electron diffusion term:

$$S_{ad} = \frac{\pi^2 k_B^2}{3e}\frac{1+\langle P\rangle}{E_F} T \ , \tag{21}$$

where the average exponent $\langle P \rangle$ of the energy dependence of the relaxation time between bands 1c and 2c varies between 0 and -1, depending on the contribution ratio of the two bands:

$$\langle P \rangle = \frac{P_1\sigma_{a,1}+P_2\sigma_{a,2}}{\sigma_{a,1}+\sigma_{a,2}} \ . \tag{22}$$

As shown below, in the energy range around 0.5 eV, where E_F is located, m_2^* for band 2c derived from Eq. (11) is smaller only by about 9% than the effective mass of band 1c calculated by Eq. (10) with $m_1^*=\hbar k_{F,1}/v_{F,1}$. Thus we can make the approximation $m_1^* \sim m_2^*$, and obtain

$$S_{ad} = \frac{2\pi^2 k_B^2 m_2^*(1+\langle P\rangle)}{3e\hbar^2 k_{F,2}^2} T \ . \tag{23}$$

In the total phonon-drag term S_{ap}, the contribution from each band involves each effective mass m_i^* and Fermi wave number $k_{F,i}$. The difference between $k_{F,1}$ and $k_{F,2}$ ($k_{F,1}<k_{F,2}$) is estimated to be about 30% around $E\sim 0.5$ eV from Eqs. (10) and (11), and the difference in the effective masses is 9% ($m_1^*<m_2^*$). Moreover, taking into account that $\sigma_{a,i}$ is proportional to the carrier density N_i, $\sigma_{a,1}/\sigma_{a,2}$ is approximated to be 0.5 from Eqs. (4) and (5). Therefore we can make the approximation $S_{ap}\sim S_{ap,2}$ in making a semiquantitative calculation.

Using Eqs. (17), (18), and (23), a least-squares fitting of the measured data is carried out in terms of the fitting parameters $k_{F,2}$, m_2^*, and L, where we take $I_c=14.2$ Å and $d=1.876$ g/cm^3 for the stage-3 NaH-GIC with a stoichiometry of C_{3a}NaH ($a\sim 4$). For boundary scattering, Rayleigh scattering, and phonon-phonon scattering, we employ the parameters for pristine graphite: $v_s=2.1\times10^6$ cm/s, $f=2.5\times10^{-12}$ cm^3/s, and $A=2.7\times10^{-5}$ cm/s K.[41] The calculated result is shown in Fig. 6 in comparison with the experimental results. Good agreement is achieved with the values $k_{F,2}=1.0\times10^7$ cm^{-1}, $m_2^*=0.12m_e$ (m_e is the free-electron mass), $\langle P\rangle=-0.90$, and $L=10\,000$ Å. From the estimated Fermi wave number $k_{F,2}$ and Eq. (11), the Fermi energy is derived to be $E_F=0.45$ eV, which is located just below the bottom of the band 3c as shown in Fig. 5. The charge-transfer rate f_c from intercalate to graphitic layer (per carbon atom) can also be estimated to be $f_c=3.7\times10^{-3}$ from the position of the Fermi energy and the relation[45]

$$E_F = \gamma_0(\sqrt{3}\pi f_c)^{1/2} \ . \tag{24}$$

The small Fermi energy and charge-transfer rate ob-

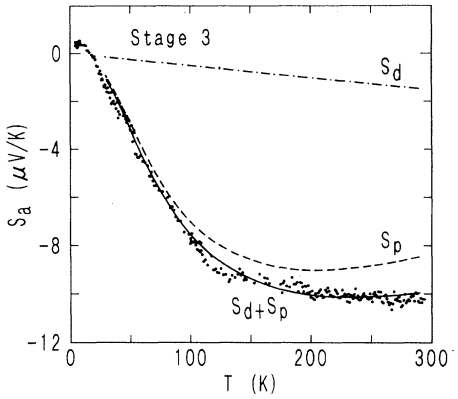

FIG. 6. Comparison of the experimental results with the calculated values obtained on the basis of Eqs. (17), (18), and (23) for the temperature dependence of the in-plane thermoelectric power S_a in a stage-3 NaH-GIC. S_d, S_p, and S_d+S_p are calculated electron diffusion term (dot-dashed line), the phonon-drag term (dashed line), and the total thermoelectric power (solid line), respectively. The least-squares fitting parameters are $k_{F,2}=1.0\times10^7$ cm^{-1}, $m_2^*=0.12m_e$, $\langle P\rangle=-0.90$, and $L=10\,000$ Å.

tained in the thermoelectric power demonstrate that the NaH intercalate does not transfer charge to the graphitic π system to the same extent as occurs for the intercalates in ordinary GIC's; that is, the presence of small Fermi surfaces for the graphitic π band is consistent with the results for the c-axis resistivity presented here. The estimated value of $\langle P\rangle=-0.9$ proves that there is a contribution from band 1c with a linear energy dispersion, which must be considered in relation to the fact that band 2c deviates from a parabolic to linear dispersion to some degree near E_F. Actually, the contribution of each band to the thermoelectric power is proportional to the conductivity, which has a quadratic k dependence. Equations (10) and (11) give $k_{F,1}^2/k_{F,2}^2\sim0.4$. Therefore band 1$c$ contributes about 30% to the total thermoelectric power. The domain size estimated at $L=10\,000$ Å is consistent with a typical size of the Daumas-Hérold domains for intercalates in GIC's.

We now discuss the stage dependence of the thermoelectric power. The absolute value of the thermoelectric power decreases with increasing stage index. This is opposite to the behavior for the stage dependence in ordinary GIC's. In ordinary GIC's, a large charge transfer between the graphite host and the guest intercalate generates relatively large cylindrical Fermi surfaces with a dimension of $k_F=10^7-10^8$ cm^{-1}. In this case, the Rayleigh scattering term having a cubic dependence on q gives the main contribution to the phonon-drag term, whose magnitude increases with decreasing stage index. From the experimental results for the in-plane thermoeletric power and c-axis resistivity, in NaH-GIC's, it is concluded that the charge transfer is almost complete within the NaH intercalates. This is due to the ionic structure having a stoichiometric composition [Na]/[H]=1, resulting in a reduction in the size of the Fermi surfaces of the graphitic π bands, as well as to the absence of conduction carriers in the NaH intercalates. The small Fermi surfaces in NaH-GIC's make the Rayleigh scattering and phonon-phonon scattering processes ineffective in the phonon-drag term. According to Eqs. (17) and (18), a saturation in S_{ap} starts at lower temperatures for a smaller Fermi wave number. This trend is revealed in the stage dependence of the thermoelectric power as shown in Fig. 2, since higher-stage compounds have smaller Fermi wave numbers due to a smaller charge-transfer rate per graphitic sheet. Therefore, in the discussion of the phonon-drag term in higher-stage NaH-GIC's, we can neglect these two contributions, resulting in the modification of Eq. (9) to yield

$$R=\frac{aq}{B+aq}\ . \tag{25}$$

In the denominator of Eq. (9), we can also neglect the term aq if we take q ($<2k_F$)$\sim10^6$ cm^{-1} and $B\sim10^{10}$ sec^{-1} for a typical domain size of $L\sim10^{-4}$ cm, that is, $R=aq/B$. In the intercalation process, the size of domains decreases with increasing stage index as expected in the Daumas-Hérold model.[38] This means that the term B becomes more important and R becomes smaller for higher-stage compounds. According to Eqs. (8) and (25), we can understand the anomalous stage dependence of the phonon-drag contribution to the thermoelectric power, which is emphasized at high temperatures in NaH-GIC's, based on the boundary scattering process.

The presence of a small positive contribution to the thermopower is observed for the in-plane S_a in the low temperature range below about 20 K. This is related to the existence of hole carriers. Though this is not clearly understood, inhomogeneity of the materials and the existence of impurity phases with different stages can give positive holes since GIC's with higher stage index than stage 3 have complicated band structures with the coexistence of positive and negative curvatures in their energy dispersion curves.[45,46]

Finally, we discuss the c-axis thermoelectric power S_c. The c-axis transport is characteristic of hopping conduction. Sugihara suggested that, even in the hopping conduction regime, the diffusion term in the thermoelectric power is expressed by a linear temperature dependence, similar to that for the band conduction system.[36] The phonon-drag effect does not contribute to the c-axis thermoelectric power.[36] The experimental finding of a linear temperature dependence in the thermoelectric power is consistent with this theoretical suggestion.

SUMMARY

We have investigated the c-axis resistivity and thermoelectric power for NaH-GIC's, and their dependence on the stage index. The c-axis resistivity shows a metallic temperature dependence, with room-temperature resistivity values around 1 Ω cm and a large residual resistivity ratio of about 0.5:1. The large magnitudes of the c-axis resistivity suggests that the c-axis transport is governed by a hopping conduction mechanism. The metallic temperature dependence is associated with the relaxation process of carriers remaining on the graphitic

planes between successive hopping events. For compounds with stages higher than stage 4, increases in the resistivity appear at low temperatures, below about 70 K. The increase in the resistivity might be ascribed to carrier localization due to lattice disorder or to interaction between the carriers and localized spins which exist in the NaH ionic intercalates in the graphitic galleries. The scattering by stacking faults can also contribute to the increased resistivity. The c-axis resistivity decreases with increasing stage index below stage 4, while an increase in the stage number above stage 4 enhances the c-axis resistivity. The stage dependence is analyzed in terms of sequential contributions of two terms: the graphene double layer unit ($\rho_{c,\mathrm{GG}}$) and the graphene-intercalate-graphene composite layer unit ($\rho_{c,\mathrm{GIG}}$). For the NaH-GIC's the ratio of $\rho_{c,\mathrm{GG}}/\rho_{c,\mathrm{GIG}}$ becomes less than unity (<0.3). This finding suggests the absence of conduction carriers in the ionic NaH intercalates. The increase in the resistivity below stage 4 is caused by the presence of nonconductive NaH spacer layers in the graphitic galleries. The increase above stage 4 is interpreted in terms of the scatterings by stacking faults which are generated more effectively in higher-stage compounds.

Thermoelectric power with negative values is suggestive of the contribution of the graphitic π conduction electrons generated by charge transfer from ionic NaH intercalates to the host graphite. The temperature dependence of the in-plane thermoelectric power is described in terms of electron diffusion and phonon-drag processes, the latter of which is governed by the relative magnitudes of the contributions from boundary scattering, electron-phonon scattering, Rayleigh scattering, and phonon-phonon scattering. The electron diffusion term gives a linear temperature dependence, while the phonon-drag term tends to saturate at high temperatures. From the analysis of thermoelectric power, we conclude that NaH-GIC's have a small Fermi surface; $k_F \sim 1.0\times10^7$ cm^{-1} with an effective mass of $m^* \sim 0.1 m_e$ for the stage-3 compound, in comparison with isostructural donor GIC's (KHg-GIC's and KH-GIC's). The stage dependence, where the increase in stage number depresses the magnitude of the thermoelectric power at high temperatures, shows a trend opposite to that for ordinary GIC's, in which Rayleigh scattering by ionized impurities plays an important role in the phonon-drag effects. The stage dependence in the thermoelectric power is explained by assuming that boundary scattering by Daumas-Hérold domains plays a crucial role. This situation can be realized in a system with small Fermi surfaces. Since the charge transfer is almost complete within the ionic NaH intercalate layer having a stoichiometric composition [Na]/[H]$\sim$1, the ionic NaH donor does not provide enough carriers to form large Fermi surfaces. The presence of positive contributions to the in-plane thermoelectric power is associated with hole carriers in an impurity phase with different stages. The c-axis thermoelectric power is attributed to an electron diffusion term governed by hopping conduction parallel to the c axis.

In conclusion, NaH-GIC's have ionic Na^+H^- intercalates with an absence of conduction carriers and a very small concentration of conduction π electrons in the graphitic planes. This is different from the situation in K^+H^- intercalates in the isostructural KH-GIC's.

ACKNOWLEDGMENTS

The authors would like to express their sincere thanks to Dr. A.W. Moore of Union Carbide for his generous gift of HOPG. We are grateful to Professor M.S. Dresselhaus for fruitful discussions. This work was supported by the Mitsubishi Science Foundation and also by the Grant-in-Aid for Scientific Research No. 02453009 from the Ministry of Education, Science, and Culture of Japan.

[1]M. S. Dresselhaus and G. Dresselhaus, Adv. Phys. **30**, 139 (1981).
[2]S. A. Solin and H. Zabel, Adv. Phys. **37**, 87 (1988).
[3]M. Collin and A. Hérold, Bull. Soc. Chim. Fr. 1982 (1971).
[4]T. Enoki, M. Sano, and H. Inokuchi, J. Chem. Phys. **78**, 2017 (1983).
[5]T. Enoki, S. Miyajima, M. Sano, and H. Inokuchi, J. Mater. Res. **5**, 435 (1990).
[6]K. Watanabe, T. Kondow, M. Soma, T. Onishi, and K. Tamaru, Proc. R. Soc. London Ser. A **333**, 51 (1972).
[7]P. Lagrange, A. Métrot, and A. Hérold, C. R. Acad. Sci. **C275**, 765 (1972).
[8]G. Alfeld and J. Völkl, *Hydrogen in Metals* (Springer, Berlin, 1978).
[9]F. D. Manchester, *Metal-Hydrogen Systems, Fundamentals and Applications* (Elsevier Sequoia, Lausanne, 1991).
[10]T. Enoki, M. Sano, and H. Inokuchi, Phys. Rev. B **32**, 2497 (1985).
[11]T. Enoki, M. Sano, and H. Inokuchi, Synth. Met. **12**, 207 (1985).
[12]T. Enoki, N. C. Yeh, S. T. Chen, and M. S. Dresselhaus, Phys. Rev. B **33**, 1292 (1986).
[13]S. Miyajima, T. Chiba, T. Enoki, H. Inokuchi, and M. Sano, Phys. Rev. B **37**, 3246 (1988).
[14]S. Miyajima, M. Kabasawa, T. Chiba, T. Enoki, and H. Inokuchi, Phys. Rev. Lett. **64**, 319 (1990).
[15]T. Enoki, K. Imaeda, H. Inokuchi, and M. Sano, Phys. Rev. B **35**, 9399 (1987).
[16]H. Yamamoto, K. Seki, T. Enoki, and H. Inokuchi, Solid State Commun. **69**, 425 (1989).
[17]T. Enoki, H. Inokuchi, and M. Sano, Phys. Rev. B **37**, 9163 (1988).
[18]L. Salamanca-Riba, N. C. Yeh, M. S. Dresselhaus, M. Endo, and T. Enoki, J. Mater. Res. **1**, 177 (1986).
[19]K. Nakazawa, K. Suzuki, T. Enoki, Y. Iye, K. Sugihara, J. T. Nicholls, and M. S. Dresselhaus, Phys. Rev. B **46**, 16 106 (1992).
[20]T. Enoki, K. Nakazawa, K. Suzuki, S. Miyajima, T. Chiba, Y. Iye, H. Yamamoto, and H. Inokuchi, J. Less-Common Met. **172-174**, 20 (1991).
[21]T. Enoki, K. Nakazawa, K. Suzuki, S. Miyajima, and Y. Iye, Mater. Sci. Forum **91-93**, 563 (1992).
[22]G. Furdin, P. Portmann, A. Hérold, and C. Zeller, C. R. Acad. Sci. **C282**, 563 (1976).

[23]M. Sano, H. Nishimura, and K. Ichimura, Synth. Met. **30**, 73 (1989).
[24]D. Guérard, C. Takoudjou, and F. Rousseaux, Synth. Met. **7**, 43 (1983).
[25]D. Guérard, N. E. Elalem, and C. Takoudjou, Synth. Met. **12**, 195 (1985).
[26]D. Guérard, L. Elansari, N. E. Elalem, J. F. Marche, and E. McRae, Synth. Met. **34**, 27 (1989).
[27]D. Guérard, N. E. Elalem, S. El Hadigui, L. Ansari, P. Lagrange, F. Rousseaux, H. Estrade-Szwarckopf, J. Conard, and P. Lauginie, J. Less-Common Met. **131**, 173 (1987).
[28]P. Lauginie, H. Estrade-Szwarckopf, B. Rousseau, and J. Conard, Synth. Met. **34**, 563 (1989).
[29]G. L. Doll, M. H. Yang, and P. C. Eklund, Phys. Rev. B **35**, 9790 (1987).
[30]T. Saito, K. Nomura, K. Mizoguchi, K. Mizuno, K. Kume, and H. Suematsu, J. Phys. Soc. Jpn. **58**, 269 (1989).
[31]S. Mizuno and K. Nakoa, J. Phys. Soc. Jpn. **58**, 3679 (1989).
[32]S. Mizuno and K. Nakao, Phys. Rev. B **41**, 4938 (1990).
[33]P. M. Chaikin and F. Kwak, Rev. Sci. Instrum. **46**, 218 (1975).
[34]T. Enoki, K. Shindo, N. Sakamoto, and K. Suzuki, Mol. Cryst. Liq. Cryst. **216**, 253 (1992).
[35]S. Ono, J. Phys. Soc. Jpn. **40**, 498 (1976).
[36]K. Sugihara, Phys. Rev. B **29**, 5872 (1984).
[37]K.Sugihara, J. Phys. Soc. Jpn. (to be published).
[38]N. Daumas and A. Hérold, C. R. Acad. Sci. **C268**, 373 (1969).
[39]P. A. Lee and T. V. Ramakrishnan, Rev. Mod. Phys. **57**, 287 (1985).
[40]M. D. Daybell, in *Magnetism V, Magnetic Properties of Metallic Alloys,* edited by H. Suhl (Academic, London, 1973), p. 121.
[41]K. Sugihara, Phys. Rev. B **28**, 2157 (1983).
[42]K. Kobayashi, H. Oshima, K. Sugihara, and T. Tsuzuku, J. Phys. Soc. Jpn. **61**, 596 (1992).
[43]F. J. Blatt, in *Solid State Physics,* edited by F. Seitz and D. Turnbull (Academic, New York, 1957), Vol. 4, p. 199.
[44]K. Sugihara (private communication).
[45]J. Blinowski and C. Rigaux, J. Phys. (Paris) **41**, 667 (1980).
[46]R. Saito, Ph.D. thesis, University of Tokyo, 1984.